An Inverse Polar Format Algorithm for Turntable Spotlight ISAR Imaging Systems Using Stepped Frequency Waveforms

Scott D. Fisher and Mark A. Richards
Georgia Institute of Technology
Atlanta, GA 30305 USA

Gregory A. Showman
Georgia Tech Research Institute
Atlanta, GA 30332-0856 USA

Abstract - **Basic turntable spotlight inverse synthetic aperture radar (ISAR) systems that employ stepped frequency waveforms implement image formation algorithms based on the premise that data collection over uniform frequency and angle steps results in a rectangular sampling of the image spatial frequency (*k*-space) domain. As a result, a simple image formation algorithm implementing only a computationally efficient inverse 2-D discrete Fourier transform (DFT) may be realized. However, this approach imposes limitations on resolution and/or scene size since the conventional data collection procedure actually results in a polar sampling of *k*-space, invalidating the rectangular grid assumption. This paper introduces a new data collection scheme using stepped frequency waveforms that are non-uniformly stepped in time and frequency so as to collect sample points according to the desired *k*-space shape. This procedure allows the use of a single inverse 2-D DFT as the image formation algorithm, thereby reducing traditional constraints on resolution and scene size while maintaining good image focus and reducing computational complexity.**

I. Introduction

Turntable spotlight inverse synthetic aperture radar (ISAR) systems use stepped frequency waveforms in order to sample the Fourier transform of a scene's reflectivity pattern at varying aspect angles. Data collection consists of transmitting a burst of simple pulses, with successive pulses having increasing frequency, at uniform steps in angle. The transmission of a large bandwidth signal provides the desired downrange resolution, while rotation of the object through a set of angles provides the desired azimuth (cross-range) resolution. The received signals are demodulated, sampled, and stored in a rectangular array in memory. These samples are then input into an appropriate image formation algorithm to create a focused image of the entire scene.

The rectangular format image formation algorithm (RFA) is the simplest imaging technique to implement due to its use of a computationally efficient 2-D inverse DFT implementation. Use of the 2-D DFT assumes that collected data samples lie on a rectangular lattice in the image spatial frequency (*k*-space) domain. This is not, however, the case. The collected data samples actually form a polar annulus in *k*-space, but under certain conditions, the 2-D DFT method provides excellent results. When these conditions are not met, this algorithm suffers from what are known as "motion through resolution cell" (MTRC) errors, which cause a spatially varying blurring of the image. MTRC errors occur when the desired image resolution becomes finer or the scene size increases in relation to the radar center frequency. Conditions under which MTRC errors are insignificant are derived in [1] and are given as:

$$\rho_x \rho_y > \frac{1}{4}\lambda_c X_S, \quad \rho_x^2 > \frac{1}{4}\lambda_c Y_S, \tag{1}$$

where X_S and Y_S are the scene diameters in azimuth and downrange, λ_c is the radar wavelength, and ρ_x and ρ_y are the azimuth and downrange resolutions.

The polar format algorithm (PFA), thoroughly discussed in [2,3], was developed to compensate for MTRC errors by implementing a downrange and azimuth interpolation step in the processing chain. The interpolations re-map the polar *k*-space sample points onto a rectangular grid so an inverse 2-D DFT will produce the desired results. However, interpolation calculations dominate processor execution time and become the main bottleneck for fast implementation. It is important to note that both the RFA and PFA algorithms also suffer from range curvature effects, but these will not be discussed in this paper and can be dismissed under the assumption that the distance r_a of the radar from the scene center is much larger than the scene extent, $r_a >> \max\{X_S/2, Y_S/2\}$.

This paper introduces the inverse polar format algorithm (IPFA), which preserves the resolution of the image while eliminating the costly range and azimuth interpolation steps used in the conventional PFA. The major innovation of the proposed algorithm is in the way that the data is collected. The use of stepped frequency waveforms has the unique advantage of being able to define specific RF frequency-angle pairs for data collection, with the collection points pre-calculated in the following way. A rectangular grid of points is laid out in *k*-space based on the desired resolution, scene size, and pixel spacing. Application of the actual polar *k*-space mapping in reverse results in a grid of non-uniform RF frequency-angle data collection pairs. A frequency agile synthesizer can then be used to collect data in the desired pattern. The *k*-space sample matching eliminates MTRC errors and only a single inverse 2-D DFT is required to form the final focused image.

II. System Model

Consider a simple turntable ISAR imaging system. The turntable is centered about the origin in the *x*-*y* plane. The azimuth coordinate is *x* and the downrange coordinate is *y*. A single point scatterer is located on the surface at coordinates (x_0, y_0, z_0), with the radar antenna at coordinates $(X_a, -Y_a, Z_a)$. The

0-7803-8234-X/04/$17.00 © 2004 IEEE

turntable rotates in a counter-clockwise direction with fixed angular rate ω_S rad/sec. During rotation, a stepped frequency waveform illuminates the turntable. In conventional stepped frequency operation, the RF frequency of the k^{th} pulse in a burst is

$$f_k = f_0 + k\Delta f, \quad k = 0...K-1, \tag{2}$$

and the transmission time for the k^{th} pulse in burst l is

$$t_{kl} = kT_s + lPT_s, k = 0...K-1, l = 0...L-1, P \geq K \tag{3}$$

Each burst is comprised of K pulses, with each pulse having the same length τ_p, and successive pulses having increasing frequency. A total of L bursts are used during the data collection, each burst having a dwell time of PT_S seconds.

On pulse number n = 0,1,...,N-1, the point target rotates to an angle $\theta_0 + n\delta\theta$, where $\delta\theta = \omega_S T_S$, and the total rotation is given as $(N\text{-}1)\delta\theta \equiv \Delta\theta$. For simplicity, let $X_a = 0$ (broadside case), and assume all point targets have negligible height contribution (z_0 = 0), resulting in a 2-D imaging model. Simple trigonometric relations provide the range to the point target location as a function of n, and a simple first-order approximation to this range expression produces

$$R[n] \approx r_a + \frac{r_0^2}{2r_a} + \sin(\phi_a)\left[x_0 \sin(n\delta\theta) + y_0 \cos(n\delta\theta)\right]. \tag{4}$$

III. Phase Analysis

The transmitted waveform for pulse kl, denoted x_{kl}, can be modeled as a complex exponential at frequency f_k with square envelope $a(t)$. The received waveform will be the superposition of the echoes from all of the scatterers on the turntable. It is thus adequate to consider the echo from the single point scatterer described earlier.

Let $R(t_{kl})$ be the range to the scatterer at the time of transmission of pulse kl. We ignore all amplitude factors from the scatterer cross-section σ, R^4 propagation loss, *etc.* since our concern is the phase structure of the received signal. After demodulation, the received baseband echo structure can be expressed as

$$y_{kl}(t) = a\left(t - t_{kl} - \frac{2R(t_{kl})}{c}\right) e^{-j\frac{4\pi f_k}{c} R(t_{kl})}. \tag{5}$$

The received signal from each pulse is sampled at a delay corresponding to the range r_a to the center of the turntable. Assuming the pulse illuminates the entire area to be imaged at once gives $a()$=1 and, arranging the samples in a k by l matrix, we obtain

$$\tilde{y}[k,l] = y_{kl}\left(t_{kl} + \frac{2r_a}{c}\right) = e^{-j\frac{4\pi f_k}{c} R[k+lP]}. \tag{6}$$

Substituting (2) and (4) into (6) results in (7), which describes the phase structure of the received data:

$$\tilde{y}[k,l] = e^{-j\frac{4\pi r_a}{c}[f_0+k\Delta f]} e^{-j\frac{4\pi}{c}[f_0+k\Delta f][x_0 \sin\phi_a \sin(k\delta\theta+lP\delta\theta)]} \cdot \ldots \cdot e^{-j\frac{4\pi}{c}[f_0+k\Delta f][y_0 \sin\phi_a \cos(k\delta\theta+lP\delta\theta)]} e^{-j\frac{2\pi r_0^2}{cr_a}[f_0+k\Delta f]} \tag{7}$$

The first phase term in (7) may be easily removed by multiplying each matrix column l by its conjugate. The last phase term is related to wavefront curvature effects, and may be dismissed under the assumption that $r_a >> r_0$. Application of a small angle approximation linearizes the second and third phase terms. Though not shown in (7), this final linearization creates an echo function that is separable in the frequency and angle variables, and is recognizable as samples of the bandlimited 2-D Fourier transform of an impulse at the target coordinates (x_0,y_0). An inverse 2-D DFT of this linearized version produces a 2-D sinc function in the image domain that is centered on the original (x_0,y_0) coordinates of the point target. Analysis of the argument of the 2-D sinc function allows several useful quantities to be calculated. Azimuth and downrange resolutions are given as

$$\rho_x = \frac{\lambda_c}{2\Delta\theta \sin(\phi_a)}, \quad \rho_y = \frac{c}{2B \sin(\phi_a)}, \tag{8}$$

with azimuth and downrange scene extents expressed as

$$X_S = \frac{\lambda_c}{2\theta_D \sin(\phi_a)}, \quad Y_S = \frac{c}{2\Delta f \sin(\phi_a)}, \tag{9}$$

where θ_D is the total rotation angle over a single dwell. Lastly, azimuth and downrange pixel spacing are defined as

$$\Delta x = \frac{\lambda_c}{2N_{DFT}\theta_D \sin(\phi_a)}, \quad \Delta y = \frac{c}{2M_{DFT}\Delta f \sin(\phi_a)}, \tag{10}$$

where M_{DFT} and N_{DFT} are the DFT sizes used for image formation.

Equation (7) is accurate so long as the total rotation angle over an entire collection period remains small. As this quantity increases, however, the linear approximations conventionally made in (7) become less valid and defocusing starts to occur. A general rule of thumb to avoid defocusing is to keep the accumulated phase error at less than $\pi/2$ radians over the given aperture. It is this condition that leads to the constraints in (1) [4]. When equal range and cross-range resolutions of ρ_0 and a scene radius of r_0 are used, (1) simplifies to the following condition [2]

$$r_0 < \frac{2\rho_0^2}{\lambda_c}. \tag{11}$$

One way to achieve finer resolutions than those imposed by the constraint of (11) is to realize that the phase structure of the second and third terms in (7) trace out a polar, not rectangular, grid of samples of the 2-D point target response in k-space. This can be seen by making use of the following definitions for the second and third phase terms of (7):

$$k_x[k,l] = \frac{4\pi}{c}\sin(\phi_a)\left[f_0 + k\Delta f\right]\left[\sin\left(k\delta\theta + lP\delta\theta\right)\right]$$
$$k_y[k,l] = \frac{4\pi}{c}\sin(\phi_a)\left[f_0 + k\Delta f\right]\left[\cos\left(k\delta\theta + lP\delta\theta\right)\right] \quad (12)$$

Neglect the $k\delta\theta$ term in the arguments of the sine and cosine for the moment. For fixed l, (12) then represents a series of samples along a line at angle $lP\delta\theta$ as k increases; that is, a set of samples evenly spaced in k-space along a radial line. When l (burst number) increases and k (frequency step number) resets, a new set of samples is traced along a new radial line. Thus, radials extend at equal angle increments of $P\delta\theta$ radians, with sample points on the radii corresponding to a particular transmitted RF frequency and spaced by $4\pi\,\Delta f\sin(\phi_a)/c$.

Closer analysis of (12) shows that the structure of the DFT frequency samples is not exactly polar. The $k\delta\theta$ term in the second sine and cosine expression gives rise to a slightly twisted or spiral polar format. For the very slow rotation rates typical of turntable ISAR, though, we can assume that the turntable will not move a significant amount between successive pulses during a burst. Under this assumption, the $k\delta\theta$ term can be neglected and the resulting pattern of frequency samples is indeed polar as just described.

Using (12) in (7) with the other simplifications discussed previously gives

$$\tilde{y}[k,l] = e^{-jx_0k_x[k,l]-jy_0k_y[k,l]}. \quad (13)$$

This equation now clearly has the form of a 2-D Fourier transform in the spatial frequency domain of a single impulse at (x_0,y_0), sampled at $k_x[k,l]$ and $k_y[k,l]$. Basic ISAR processing would produce the desired results if the k-space sample points lay on a rectangular grid. Since (12) shows that these samples lay in a polar grid, use of a 2-D DFT with its implied rectangular sample grid to form the image will produce defocusing effects, the magnitude of which depends on the amount of accumulated phase error.

The PFA counteracts these effects by linearly interpolating the polar k-space sample points onto the desired rectangular grid. The next section will detail a modified algorithm that uses stepped frequency waveforms to exploit the RF frequency-angle paired sample locations of the collected data in order to eliminate the PFA interpolation steps, while still maintaining resolution and scene size requirements.

IV. Modified Algorithm

By exploiting the one-to-one relationship between the RF frequency-angle sample points of the data collection process and the k-space sample points of the received data, it is possible to remove the two interpolation steps and still produce imagery with comparable resolution to those produced implementing the PFA. Specifically, if the data were collected in an appropriate "inverse polar" grid of RF frequency-angle samples, the transformation in (12) would place the new data points on a rectangular k-space grid, which could readily be used in an inverse 2-D DFT. The necessary RF frequency-angle pairs can be determined by pre-calculating the desired rectangular grid of points in k-space using (8)-(10), and then subsequently determine the corresponding RF frequency-angle pairings using the inverse of the transformation (12):

$$f_{kl} = \frac{c}{4\pi\sin(\phi_a)}\sqrt{k_x^2[k,l] + k_y^2[k,l]}$$
$$\theta_{kl} = \tan^{-1}\left(\frac{k_y[k,l]}{k_x[k,l]}\right). \quad (14)$$

By using stepped frequency waveforms, one can easily set up a schedule of pulse frequencies to match the required RF frequency-angle pairings obtained from (14) for the modified, nonuniform data collection scheme. An agile frequency synthesizer is now required in order to generate the complex, nonuniform sequence of pulse frequencies and timings. The resolution, accuracy, and settling time of the synthesizer and RF hardware will determine how accurately the desired frequency schedule can be generated.

V. Simulation Results

A MATLAB© simulation was run using equal azimuth and downrange resolutions of 0.25 meters before windowing for an image patch size of 20 meters by 20 meters. Hamming weighting was used to reduce sidelobe levels. The radar was located at a range of Y_a = -1000 m from the turntable center. Fig. 1a shows the location of sample points for data collected in the traditional rectangular format, which have equal spacing between frequency and angle bins. Fig. 1b shows the polar pattern of sample points in k-space when the transformation in (12) is applied to the data in Fig. 1a. Fig. 2a shows the image formed by taking the inverse 2-D DFT of the data in Fig. 1b. The inscribed circle in the plot, calculated from (11), shows the maximum radius of a scene that can be imaged before defocusing occurs. Noticeable effects are seen in point targets located outside of the inscribed circle, with the worse defocusing occurring in point targets at the scene corners.

Fig. 3b shows the rectangular grid of k-space points that is pre-computed for use with the modified algorithm based on scene size and resolution requirements. Fig. 3a shows the corresponding "inverse polar" format RF frequency-angle data collection pairs that are obtained when the sample points from Fig. 3b are input in the inverse transformation given in (14). Fig. 2b is the image formed by an inverse 2-D DFT of the polar format data in Fig. 3a. Compare Figs. 1a and 1b to 3a and 3b, and the image in Fig. 2a to that in Fig. 2b.

The image in Fig. 2b clearly does not suffer the defocusing effects seen in Fig. 2a. The modified algorithm has been able to effectively remove these errors, while still being able to image a scene of the same size and maintain the same resolution. This image is also comparable to what would be obtained if the data in Fig. 1b were interpolated onto a rectangular grid of sample points before an inverse 2-D DFT was performed, *i.e.* if the PFA was used.

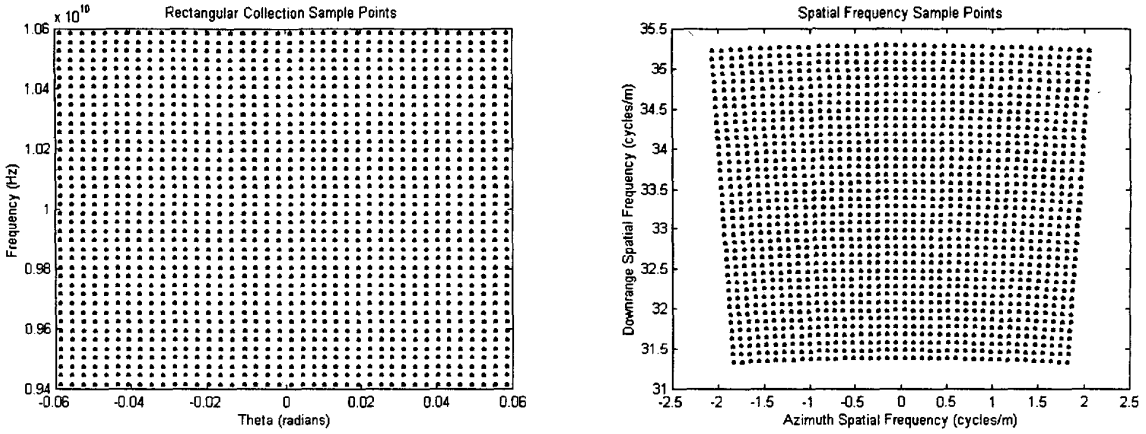

(a) (b)

Fig. 1. (a) Rectangular data collection points. (b) Polar spatial frequency points.

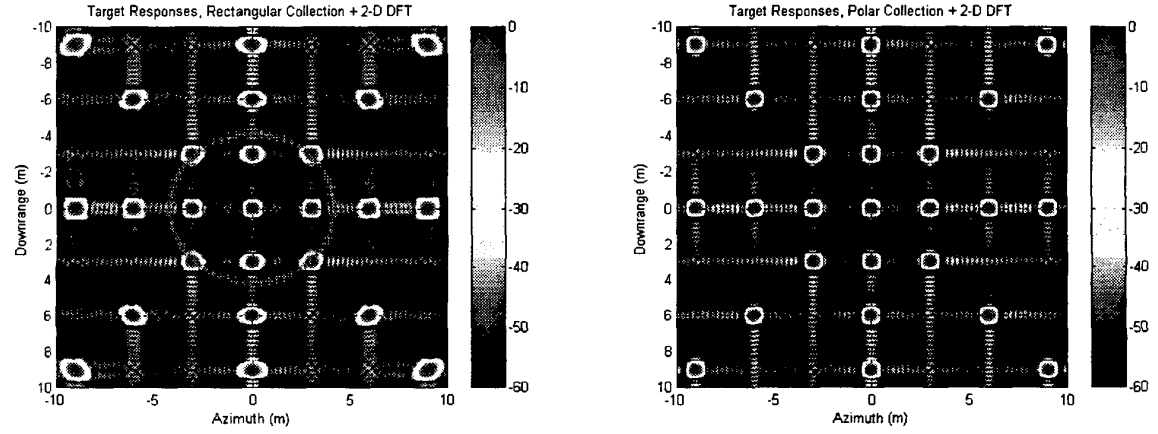

(a) (b)

Fig. 2. (a) 2-D DFT image formed from rectangular data collection. (b) 2-D DFT image formed from "inverse polar" data collection.

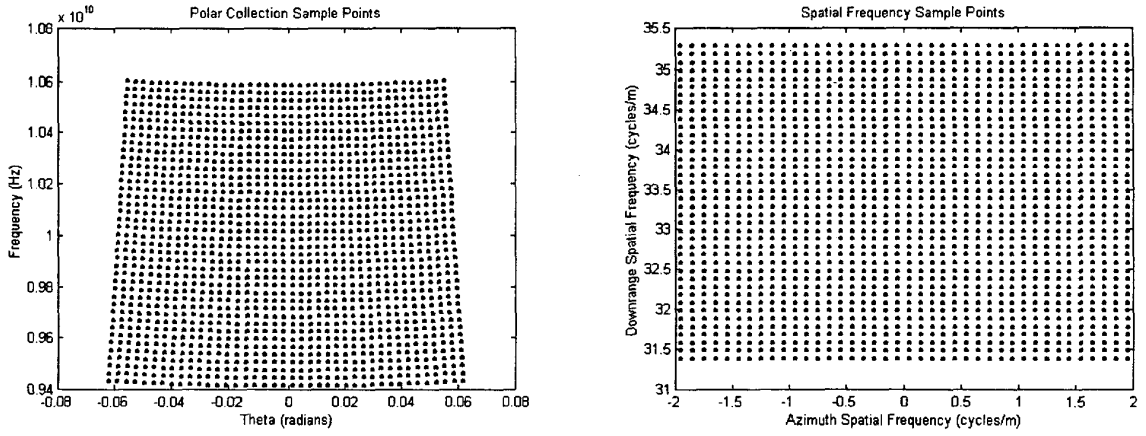

(a) (b)

Fig. 3. (a) "Inverse polar" data collection points. (b) Rectangular spatial frequency points.

The generated grid of RF frequency-angle data collection points in Fig. 3a still needs to be converted to an implementable sampling schedule. Stopping, starting, and reversing the turntable to rotate it to various angular positions is not a viable option since very large and heavy objects (*e.g.* tanks, transport vehicles) are usually imaged in this kind of system. It is therefore necessary to let the turntable run continuously. Consequently, the RF frequency-angle pulse pairs should be transmitted in order of increasing angle, with the pulse frequency and timing varied as necessary while the turntable rotates. Fig. 4 shows the beginning portion of the sampling schedule after the frequency-angle pair samples from Fig. 3a have been sorted and re-plotted.

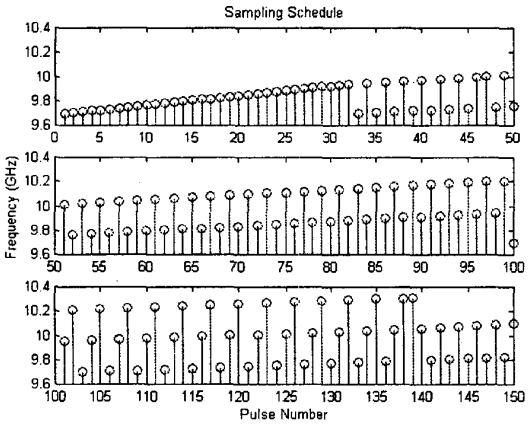

Fig. 4. Sampling schedule.

VI. Metric Comparison

This section presents a basic metric comparison based upon the simulations in the previous section to show how improved resolution may be gained through using the IPFA. Fig. 5a shows downrange and azimuth cross-sections of the center target and Fig. 5b shows the downrange and azimuth cross-sections of the corner target for the rectangular format image formation algorithm. Similarly, Fig. 6a shows the downrange and azimuth cross-sections of the center target and Fig. 6b shows the downrange and azimuth cross-sections of the corner target for the IPFA.

Note that there is very little difference between Fig. 5a and Fig. 6a. This is expected, as the center target is the only one that experiences no motion relative to the radar platform. The resolution (3dB mainlobe width) is roughly 0.36 meters, the mainlobe null-to-null width is approximately 1 meter, and the peak sidelobe level is approximately –42dB. These values match very well with what we would expect once the Hamming weighting is taken into consideration.

This is not the case for scatterers located away from the turntable center. Fig. 5b shows severe resolution loss for the corner target. In fact, the reflector shows an azimuth mainlobe spread twice that of the center target, and a downrange mainlobe spread 1.5 times that of the center target. This spreading is the result of accumulating MTRC phase errors; the smearing effect was also readily apparent in the image of Fig. 2a.

Fig. 6b shows that the modified algorithm does a much better job of focusing targets at the far edge of the imaging area. There is essentially no cross-range or downrange mainlobe spreading compared to the center target, although Fig. 6b does exhibit a slightly higher peak sidelobe level. Smearing effects have therefore been greatly reduced, resulting in a much better focused image.

VII. Conclusions

This paper introduced a new turntable ISAR algorithm that provides image quality comparable to that achieved through the use of the PFA, with only the implementation of a single inverse 2-D DFT, and without the costly azimuth and downrange interpolations. By matching the *k*-space sample points to the inverse 2-D DFT and then using an inverse polar format transformation to generate a set of nonuniform RF frequency-angle data collection points, phase errors leading to spatial defocusing can be corrected. In essence, this method seeks to match the collection scheme to a given algorithm, vice matching the algorithm to the collection scheme, *i.e.* the rectangular and PFA algorithms.

By using stepped frequency waveforms, we can take advantage of the known relationship between the RF frequency and angle for a given pulse. Since the resulting RF frequency-angle sample pairs do not follow a normal constant PRF, linear frequency ramp pattern, a more complicated nonuniform data collection scheme must be implemented. This scheme involves generating a sampling schedule from the RF frequency-angle pairings and using a frequency synthesizer to illuminate the image area with the proper frequency at each angle. This is a significant change from current turntable ISAR systems. However, the gain of having matched the algorithm sampling scheme to the 2-D DFT while maintaining resolution comparable to that obtained with the more complex PFA, may make this increase in transmitter complexity worthwhile.

VIII. Future Work

There are still several areas that need to be investigated relating to the application of this new algorithm. First, the effects of wavefront curvature need to be examined and, if possible, corrected.

Second, waveform control quantization effects must be taken into account when determining the accuracy of the frequencies that can be transmitted using a frequency synthesizer. Arbitrarily precise RF frequencies and sample angles can be generated in a simulation, but real frequency synthesis hardware is limited in its frequency accuracy and settling time. This limited precision needs to be investigated to determine its effects on image focusing and resolution.

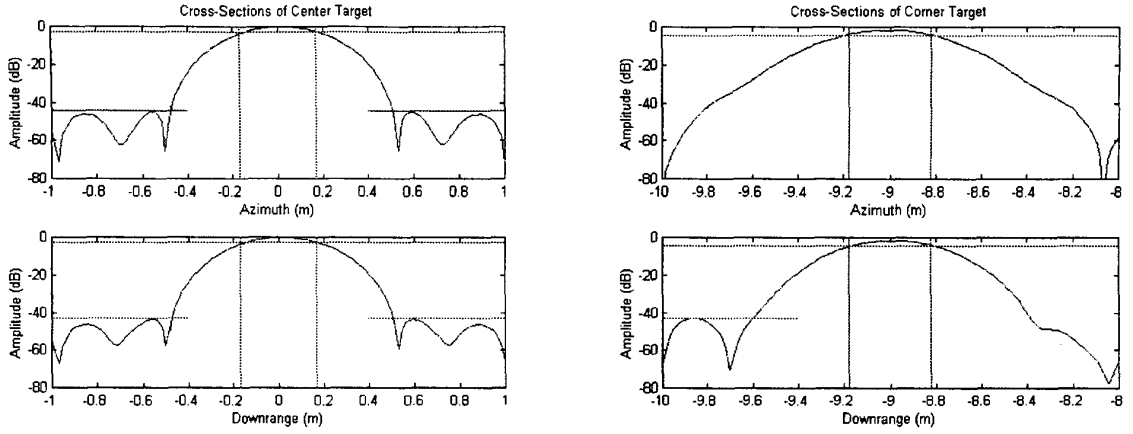

(a) (b)

Fig. 5. (a) Azimuth and downrange cross-sections of center target for the RFA. (b) Azimuth and downrange cross-sections of corner target for the RFA.

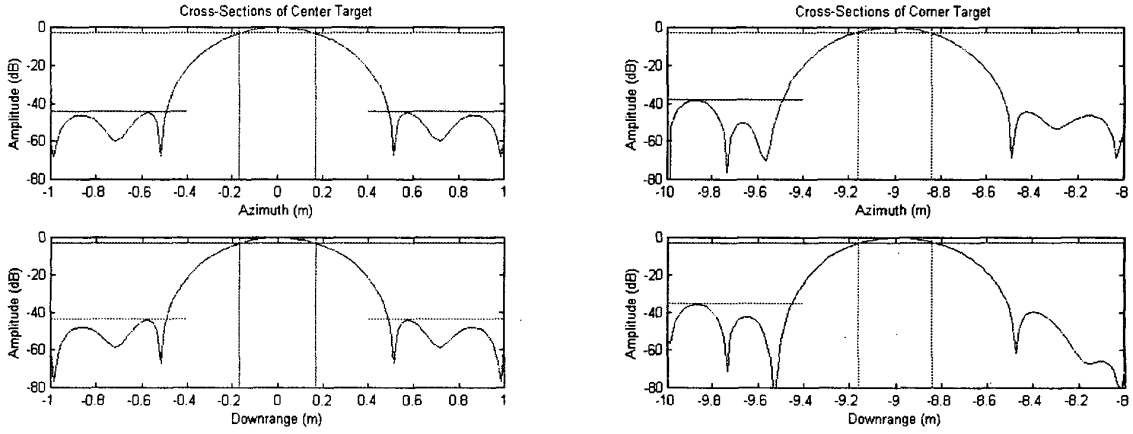

(a) (b)

Fig. 6. (a) Azimuth and downrange cross-sections of center target for the IPFA. (b) Azimuth and downrange cross-sections of corner target for the IPFA.

Third, a performance measure and cost analysis is needed to determine if the new imaging algorithm provides any system benefits over existing approaches. Removing the range and cross-range interpolation step will certainly speed up processor and algorithm performance, but at the cost of a frequency synthesizer with specialized timing schedules.

Fourth, the effect of turntable motion between successive pulses should be investigated. This paper assumed that turntable rotation was so small between successive pulses that it could be ignored. The magnitude and effect of this term for realistic system parameters should be determined. If significant, it should be determined if it is possible to extend the inverse transformation to include this effect.

Lastly, the periodicity of the sample schedule should be investigated. In conventional operation, the turntable rotates through a full circle while data is collected continuously using the periodically repeating linear ramp frequency stepping. The target can be imaged from any aspect angle by simply selecting the data taken at angles around the aspect angle of interest. The nonuniform sampling scheme suggested here does not appear to repeat periodically. This characteristic will place some limits on the ability to perform continuous imaging at arbitrary aspect angles.

REFERENCES

[1] W. M. Brown, and R. J. Fredricks, "Range-Doppler imaging with motion through resolution cells," *IEEE Transactions on Aerospace and Electronic Systems*, vol. AES-5, no. 1, January 1969, pp. 98-102.

[2] W. G. Carrara, R. S. Goodman, and R. M. Majewski, *Spotlight Synthetic Aperture Radar*. Artech House, Norwood, Massachusetts, 1995.

[3] C. V. Jakowatz, Jr., *et al*, *Spotlight-Mode Synthetic Aperture Radar: A Signal Processing Approach*. Kluwer, Boston, Massachusetts, 1996.

[4] J. L. Walker, "Range-Doppler imaging of rotating objects," *IEEE Transactions on Aerospace and Electronic Systems*, vol. AES-16, no. 1, January 1980, pp. 23-52.